Multi-Patch Integrodifference Models and Their Eigenvalue Problems in Spatial Ecology

by

Ali Beykzadeh

Master of Science, University of New Brunswick, 2020
Master of Pure Mathematics, Ferdowsi University, 1997
Bachelor of Science in Mathematics, University of Birjand, 1995

A Dissertation Submitted in Partial Fulfilment of
the Requirements for the Degree of

Doctor of Philosophy

In the Graduate Academic Unit of Mathematics and Statistics

Supervisor:	James Watmough, PhD, Dept. of Mathematics and Statistics
Examining Board:	Myriam Barbeau, PhD, Dept. of Biology Lin Wang, PhD, Dept. of Mathematics and Statistics Branimir Ćaćić, PhD, Dept. of Mathematics and Statistics
External Examiner:	Xiao-Qiang Zhao, PhD, Dept. of Mathematics and Statistics, Memorial University

This dissertation is accepted by the
Dean of Graduate Studies

THE UNIVERSITY OF NEW BRUNSWICK

October, 2024

Abstract

In the realm of spatial ecology, we grapple with fundamental questions: How can we design effective nature reserves to safeguard the survival of species? In the context of fisheries, how wide can a fishing zone be without compromising the stability of fish populations? These inquiries have fueled my motivation to delve into the subject matter of this thesis. While we acknowledge that precise answers to such questions remain elusive, I have endeavored to contribute to our understanding of these critical issues.

Our journey begins with an exploration of integrodifference equations (IDEs) in spatial ecology in Chapter 1. These mathematical models serve as powerful tools for unraveling the intricate spatial and temporal dynamics of populations characterized by discrete generations and continuous spatial domains.

Imagine a population confined to a single isolated patch — a scenario akin to a lake surrounded by hard boundaries. Within this patch, there exists a gap devoid of reproduction, effectively separating the population. Consider, for instance, a protected fishing zone within a lake. Our focus in Chapter 2 lies on understanding the persistence of such populations. We model their life cycles using IDEs and present a method to calculate the maximum allowable gap size that ensures population persistence.

The concept of critical patch size takes center stage in Chapter 3. It refers to the minimum favorable area below which a population faces the risk of extinction.

Our investigation accounts for the demographic and dispersal traits of individuals, recognizing that these traits may vary across patches. Surprisingly, we find that the smallest critical patch size occurs when individuals exhibit a propensity to leave the patch. Conversely, the largest critical patch size arises when boundaries are more restrictive, limiting the chances of individuals leaving the patch.

In the patchy landscape, Chapter 4 introduces an approximation method that simplifies equilibrium population calculations. Our approach involves a form of the redistribution approximation tailored for piecewise continuous kernels. The accuracy of our estimate improves as movement biases near patch boundaries intensify. Key factors influencing our estimate include the growth term's derivative and the deviation of the equilibrium solution from its average across patches

Dedication

To my wife, Rashel, whose patience and sacrifices have been the backbone of my success. Thank you for standing by me through every challenge.

Acknowledgements

I would like to express my deepest gratitude to my advisor, Dr. James Watmough, for his continuous support, patience, and invaluable guidance throughout my research. His expertise and encouragement have been instrumental in the completion of this work.

I also appreciate the help of the administrative and technical staff at the University of New Brunswick. Their support and assistance have been crucial in navigating the various challenges of this journey.

To my family and friends, thank you for your unwavering support, encouragement, and understanding. Your belief in me has been a constant source of strength and motivation.

To my wife, Rashel, your love and support have been my anchor. Thank you for believing in me, for your endless patience, and for standing by me through every high and low. Your presence has made this journey possible.

I would also like to acknowledge Dr. Frithjof Lutscher, whose work has been a source of inspiration and motivation. His contributions to the field have greatly influenced my own research.

Table of Contents

List of Figures

List of Notation

a	scaled factor in growth function
x	settlement point
y	release point
t	time
m	number of bounded patches
Ω_i	i^{th} patch
R	growth rate at low density, $R = F'(0)$
κ_i	the carrying capacity in Ω_i
r_i	the intrinsic growth rate in Ω_i
σ^2	variance of the Gaussian kernel
ν_i	diffusion coefficient within patch Ω_i
α_i	per capita settling rate within patch Ω_i
β_i	per capita death rate within patch Ω_i
μ_i	dispersal decay rate within patch Ω_i
a_i	patch boundary between Ω_i and Ω_{i+1}, (interface point)
z_i	bias at the interface point a_i
δ	Dirac delta function
k	dispersal kernel
k_L	Laplace kernel
N	population density
F	growth function
I	identity matrix
$\mathcal{A}$	non-linear operator
λ	eigenvalue
ϕ	eigenfunction
L	length
l	gap size
u_j	dispersal redistribution function
U_{ij}	spatial average of the redistribution function

Chapter 1

Integrodifference equations in spatial ecology

This thesis explores the dynamics of spatial ecology through the lens of an integrodifference equation, a mathematical model that encapsulates two fundamental aspects: the population growth function and the dispersal kernel for populations with a specific life cycle. The growth function represents the local dynamics of a population, encompassing elements such as birth, death, and competition. In contrast, the dispersal kernel outlines the probability of an individual relocating from one location to another within each generation. By integrating these components, we delve into ecological concepts like critical patch size, which arise from the interplay between population growth and dispersal. Furthermore, we investigate the existence and characteristics of the steady-state and propose a method for its approximation using the dispersal success function. This chapter serves as a foundation for the subsequent chapters, which focus on critical gap size, critical patch size, and redistribution approximation.

1.1 Integrodifference equations in spatial ecology

Integrodifference equations are a type of mathematical model that can capture the spatial and temporal dynamics of annual seed plants or insects, among other organisms [10]. These particular organisms have a distinct life cycle that consists of two phases: a growth phase and a dispersal phase. In the growth phase, they develop from seeds or eggs to mature individuals that produce offspring. In the dispersal phase, they move to new locations where they overwinter or remain dormant until the next season. Integrodifference equations are useful for studying the effects of environmental processes, such as climate change or habitat fragmentation, on the spatial spread and persistence of annual plants or insects. For example, integrodifference equation models have been formulated for annual plant populations without a seed bank to study how intraspecific competition acts to reduce vital rates [16].
An Integrodifference equation (IDE),

$$N_{t+1}(x) = \int_{\Omega} k(x,y)F(N_t(y),y)dy, \tag{1.1}$$

describes how a population evolves in discrete time and continuous space. It assumes that individuals first reproduce according to a growth function, then disperse according to a dispersal kernel. To formulate an IDE, let Ω be a collection of non-overlapping intervals, Ω_i, of the real line. Population density at the beginning of the growth phase in year $t \in \{0, 1, 2, \dots\}$ is denoted by $N_t : \Omega \to \mathbb{R}$. And $F : \mathbb{R} \times \Omega \to \mathbb{R}$ is the (possibly piecewise) population density at the end of the growth phase in year t. The dispersal kernel, k, models movement between points in Ω, $k : \Omega \times \Omega \to \mathbb{R}$. Specifically, $k(x, y)$ is the probability density for dispersal to $x \in \Omega$ conditional on the starting position $y \in \Omega$. The spatial variable x represents the location of a disperser at the end of the dispersal phase, while y represents the location of a disperser at the beginning of the dispersal phase.

1.1.1 Growth functions

We begin by discussing population growth in a single homogeneous patch and simplifying (1.1) to a simple difference equation in one real variable. The growth function F, with the recursion

$$N_{t+1} = F(N_t), \tag{1.2}$$

represents how the population density changes over time due to processes such as reproduction, competition, predation, and environmental variability. Different growth functions have different properties and implications for the stability and persistence of the population. We choose the growth function based on the life cycle of the organism, and the ability to produce an abundance of offspring, i.e., new growth. Another useful quantity is the per-capita growth rate, $F(N)/N$, which measures the average number of offspring produced by each individual. The per-capita growth rate indicates whether the population is increasing ($F(N)/N > 1$), decreasing ($F(N)/N < 1$), or staying constant ($F(N)/N = 1$). In this section, we explore three common types of growth functions that model different scenarios of population change: linear, Beverton-Holt, and Ricker.

Linear growth, $F(N) = RN$, assumes the per-capita number of offspring is R, independent of population density. This means that the population grows exponentially at a constant rate R. The only steady state is $N^* = 0$ unless $R = 1$, where the population is extinct. To find the general solution for the population size at time t, we use the recursion in (1.2) with the linear growth function. This gives us $N_t = R^t N_0$, where N_0 is the initial population size. A constant per-capita growth function, assumes that each individual contributes the same amount to the overall growth rate regardless of the population size. However, this function has some limitations and drawbacks. Depending on the value of R, the growth factor, the population may exhibit exponential growth ($R > 1$) or decay ($0 < R < 1$). A constant per-capita

growth function does not capture the effects of population interactions, such as competition or predation, that may affect the growth rate. An approach is to use nonlinear growth functions that account for these processes.

The Beverton-Holt growth model, denoted by

$$F(N) = \frac{R}{1 + aN} N, \quad R, a > 0$$

is a widely accepted model for describing the recruitment dynamics of renewable resources such as fish stocks [21]. This model is a nonlinear population growth function, making it particularly useful for modeling populations that are influenced by demographic factors. The model posits that the per-capita number of offspring decreases with increasing population density, scaled by a factor of a, as individuals compete for limited resources like food or space. The environment's carrying capacity, represented by

$$\kappa = \frac{R - 1}{a},$$

is dependent on both a and R. This is because $F(N) > N$ for $0 < N < \kappa$, and $F(N) < N$ for $N > \kappa$, indicating that the population growth changes based on the carrying capacity of the environment.

The Ricker growth model, $F(N) = Ne^{r(1-aN)}$, where $a, r > 0$, also known as the Ricker curve or Ricker model, was developed by Bill Ricker in 1954 to study the relationship between stock and recruitment in fisheries. The model assumes that the per-capita growth rate of the population decreases, scaled by a factor of a, exponentially with its density. In the Ricker growth model, r is a positive parameter that determines how quickly the population grows when its size is small relative to the carrying capacity of the environment.

Both the Beverton-Holt and Ricker models have two fixed points when $R > 1$, (Figure 1.1), noting that $R = \exp(r)$ connects r and R. For both models, these are at

$N = 0$ and the interior equilibrium, N^*. The threshold $R > 1$ is necessary for the existence of the interior equilibrium in both models. In the Beverton-Holt model, the interior equilibrium is stable, which means that if the population size deviates slightly from N^*, it will return to N^* over time. On the other hand, in the Ricker model, the interior equilibrium is typically unstable due to overcompensation, leading to oscillations or chaotic dynamics. The Beverton-Holt model exhibits saturation, where the per-capita growth rate decreases as the population size increases, eventually stabilizing at the carrying capacity. In contrast, the Ricker model exhibits overcompensation, where the population size overshoots the carrying capacity and then decays to zero, leading to oscillations or chaotic dynamics.

1.1.2 Dimensional analysis

Non-dimensionalization is a technique that simplifies the analysis of a mathematical model by eliminating the physical units of the variables and parameters. By introducing a constant κ with the same dimensions as N_t, we can define a dimensionless variable n_t such that $N_t = \kappa n_t$. This reduces the number of parameters in the model and makes it easier to compare different cases or scenarios.

For example, in the Beverton-Holt growth we will find

$$n_{t+1} = \frac{Rn_t}{1 + a\kappa n_t}$$

In this context, one might say that choosing $\kappa = 1/a$ serves to have a particularly simple form of the denominator whereas choosing $\kappa = (R-1)/a$ gives a particularly simple form of the positive fixed point, $n = 1$. As discussed in Section (1.1.1), the latter choice requires $R > 1$, and the model only has one equilibrium if $R < 1$, see Figure 1.1.

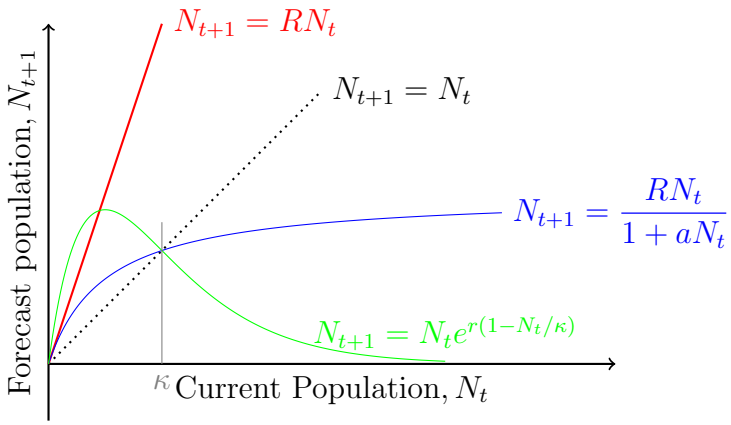

Figure 1.1: The Beverton-Holt reproduction function, blue, has two fixed points when $R > 1$. But the only steady state of linear growth function, red, is $N^* = 0$. The Ricker model, green, has also two fixed points.

1.1.3 Dispersal kernels

The dispersal kernel, k, in Equation (1.1) is a useful tool to study, for example, how plants spread across a landscape. It represents the likelihood of finding a plant or a seed at a certain distance from its source. The shape and size of the dispersal kernel can have important implications for plant population dynamics and conservation [17]. The dispersal phase is a stage in the life cycle of some organisms when they relocate from one location to another. A prerequisite for successful distribution is the ability to leave a habitat at all. The dispersal kernel k can be used to model the spatial spread and genetic diversity of populations, as well as the potential impact of environmental factors on dispersal patterns . The dispersal kernel, $k(x, y)$, describes the probability density of an individual born at location y settling at location x.

In this context, the dispersal kernel represents the combined effects of all the processes that influence the movement and settlement of offspring, such as their innate dispersal abilities, environmental factors, and social interactions. By incorporating this kernel into a population model, we can account for the spatial structure of the population and study how it affects its growth and dynamics.

The kernel $k(x, y)$ must be non-negative for all x and y. If dispersal involves mortality

or if some individuals disperse outside the domain of interest, Ω, then we have the following inequality.

$$\int_{\Omega} k(x,y)dy \leq 1$$

The inequality indicates that that some individuals are lost from the population due to dispersal. An example of this situation is the wind dispersal of seeds from plants on an island, where some seeds may land in the water so that will not germinate.

The Gaussian kernel or Normal distribution in one spatial dimension has the following form.

$$k(x,y) = \frac{1}{\sqrt{2\pi\sigma^2}} \exp\left(-\frac{(x-y)^2}{2\sigma^2}\right) \tag{1.3}$$

The Gaussian kernel has some properties, such as being smooth, symmetric, and defined for all real numbers, Figure 1.2. This means that it is a continuous function with no sharp edges, and it is symmetrical around its center. The Gaussian kernel plays a crucial role in ecological modeling and analysis. It is commonly used to describe spatial interactions, resource utilization, and species distributions [10]. Specifically, ecologists often apply the Gaussian kernel to model how organisms interact with their environment, such as seed dispersal, habitat suitability, and population dynamics.

The Gaussian kernel also captures the concept of resource utilization. When organisms compete for limited resources (e.g., food, space, or nutrients), their utilization patterns can be approximated by a Gaussian distribution. For instance, consider plant species competing for light, nutrients, or water. The Gaussian kernel characterizes how their resource use declines as they move away from their optimal niche position. The smoothness and symmetry properties of the Gaussian kernel are ecologically relevant. The Gaussian kernel ensures that resource utilization smoothly transitions from one point to another. This property aligns with ecological processes where gradual changes occur across landscapes. The symmetry around the center re-

flects the balanced competition between species. It implies that species with similar resource requirements interact more intensely, while distant species have weaker interactions. The Gaussian kernel's infinite support means that it extends indefinitely along the resource axis. Ecologically, this represents the potential for long-distance interactions. For example, consider pollen dispersal by wind. The Gaussian kernel captures the probability of pollen reaching distant locations, affecting genetic diversity and population dynamics. While the Gaussian kernel is widely used, it is essential to recognize its limitations. Small deviations from the Gaussian shape can lead to different ecological outcomes. Ecologists should explore alternative kernels (e.g., heavy-tailed kernels) to account for specific ecological scenarios. These deviations may result from secondary ecological mechanisms or numerical model implementations [1].

Although a common choice of dispersal kernel is the Gaussian kernel, which assumes that the dispersal probability decreases exponentially with the square of the distance, this kernel may not fit well with some empirical data, such as those from insect studies [17], which show a slower decay of dispersal probability with distance. A different dispersal kernel that can capture this slower decay is the Laplace kernel, Equation (1.4), also known as the back-to-back exponential kernel. The Laplace kernel has a heavier tail than the Gaussian kernel and is often used in mathematical models of dispersal.

$$k(x,y) = \frac{1}{\sqrt{2\sigma^2}} \exp(-\sqrt{\frac{2}{\sigma^2}}|x-y|) \tag{1.4}$$

We may want to simplify the notation in (1.4) and write the Laplace kernel with dispersal parameter $a = \sqrt{\frac{2}{\sigma^2}}$. The quantity $1/a$ has units length and denotes the mean absolute deviation or mean dispersal distance.

The choice of the Laplace kernel is motivated by its ability to capture the slower decay in dispersal processes, which is often observed in natural phenomena (Figure 1.2). Unlike the Gaussian kernel, which assumes that most dispersal events occur

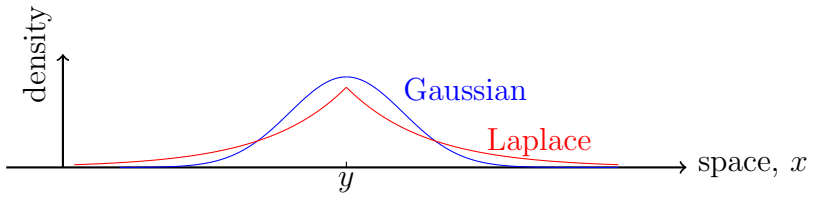

Figure 1.2: Laplace kernel, red, shows a slower decay of dispersal probability with distance than Gaussian, blue.

close to the point of origin and rapidly decreases in probability with distance, the Laplace kernel allows for a heavier tail, indicating a significant probability of long-distance dispersal events.

Examples of the use of the Laplace kernel in dispersal models include modeling seed dispersal in plant ecology, where seeds may be dispersed over a range of distances due to various biotic and abiotic processes [6]. As well as describing the spread of pollutants in an aquatic environment, where the Laplace kernel can represent the long-range transport of particles due to currents [23].

While the Laplace and Gaussian kernels are renowned for their utility in these domains, they represent merely a fraction of the kernels employed by ecologists and evolutionary biologists. The seminal works of Abrams [1], Ackermann and Doebeli [2], and Baptestini et al. [3] demonstrate the application of a diverse array of kernels in modeling ecological systems.

Abrams [1] delved into the theory of limiting similarity, which necessitates kernels that capture the intricate structure of resource distribution and interspecies competition. This approach allows for a more granular analysis of how similar two competing species can be before one is competitively excluded. Ackermann and Doebeli [2] investigated the breadth of ecological niches and the ensuing adaptive diversification. They posited that kernels reflecting the phenotypic distribution within populations can significantly influence evolutionary trajectories, thereby shaping the adaptive landscape. Furthermore, Baptestini et al. [3] scrutinized how the form of competi-

tion and carrying capacity kernels can sway the propensity for disruptive selection. Their research suggests that non-conventional kernels can shed light on the conditions conducive to species diversification and the maintenance of polymorphisms within populations. These studies collectively highlight the imperative of incorporating a spectrum of kernels beyond the conventional Laplace and Gaussian forms. By integrating kernels that encapsulate the complexities of ecological interactions and evolutionary dynamics, researchers can attain a more nuanced comprehension of the mechanisms underpinning biodiversity and the coexistence of species.

1.2 Discussion

This chapter provides an overview of the main ideas and applications of integrodifference equations in spatial ecology. These mathematical models are useful for understanding the spatial and temporal dynamics of populations that have discrete generations and continuous space. They consist of a growth function that describes the local dynamics of the population and a dispersal kernel that describes the movement of individuals between locations. These models can help us understand how ecological processes such as critical patch size arise from the interactions between population growth and dispersal.

Integrodifference equations have been applied in theoretical ecology to address various questions related to conservation biology, biological invasions, structured populations, and spatial variation. These models have revealed the mechanisms that drive population dynamics and have helped to inform management strategies for conserving threatened species and controlling invasive species.

However, there are still many challenges and open questions in the field of spatial ecology that can be tackled using integrodifference equations. For instance, there is a need for more research on how environmental factors such as climate change or

habitat fragmentation affect the spatial spread and persistence of populations, or how individual movement response to habitat edges effects population persistence and spatial spread, [12] . There is also a need for more work on developing efficient numerical methods for solving integrodifference equations and for incorporating more realistic biological mechanisms into these models.

Chapter 2

Critical gap size

This study explores the persistence of a population within a single patch with hard boundaries, such as a lake, implying that no disperser exits the habitat. A centrally located non-reproductive gap, divides the population within the patch. We present a method to calculate the maximum size of this gap for which the non-zero steady-state is stable. The population's life cycle is modeled by a one-dimensional domain integrodifference equation (IDE). This approach separates the reproduction phase from the dispersal phase in the species' life cycle. For selected parameter values, we found that when individuals are more likely to settle in the fishing zone, or when spend more time there, the fishing area must be shorter, and the no-take length must be larger to maintain the population in the lake. The relationship between the reproduction rate of the species in the no-take area and the optimal length of the fishing zone indicates that a longer fishing zone requires a higher reproduction rate in the no-take area to sustain the total population in the lake. This ensures that the no-take sides of the lake can support each other and prevent population collapse.

2.1 Introduction

This chapter focuses on the persistence of a population that lives in a single isolated patch with hard boundaries, such as a lake. We assume that the population cannot leave the patch and that there is a gap, with no reproduction, in the middle of the patch that separates the population. For example, the gap could be a fishing zone in a protected lake. The population we consider has a life cycle that can be modeled by an integrodifference equation (IDE). We present a method to calculate the maximum gap-size that allows the population to persist.

One way to protect a species from overfishing in a lake is to create a no-take reserve, which can be the lake with no gap in the middle where fishing is prohibited. No-take reserves have been shown to increase the density and diversity of organisms inside them, compared to partially protected areas nearby [8]. However, no-take reserves also have some drawbacks, such as reducing the fishing opportunities for local communities and creating conflicts with extractive users. Therefore, some managers prefer to use marine reserves with less strict regulations, which allow some fishing activities in certain zones [20].

To determine the optimal size of the fishing zone, we simplify the problem to a one-dimensional domain IDE, in which the reproduction phase of the species' life cycle is separated from the dispersal phase. We assume that the total length, L, of the reserve is given, and we want to find largest length of the fishing zone, l which permits persistence, and to study how population size depends on l. We will derive a formula for l based on the parameters of the species' demography and dispersal.

2.2 Method

The whole real line is considered as the domain Ω , and is divided into five sub intervals Ω_j, for $j \in \{0, 1, 2, 3, 4\}$, as shown in the following diagram.

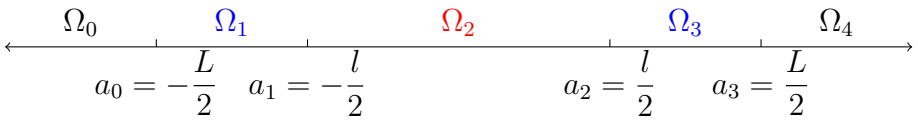

Figure 2.1: In a one-dimensional space in which, an unfavorable patch, Ω_2 is located between two favorable patches Ω_1 and Ω_3, has created a gap in the domain.

Ω_2 represents the gap between no-take regions Ω_1 and Ω_3, and the semi-infinite subsets Ω_0 and Ω_4 are the exterior regions of the lake.

The settling rate, the death rate, and the motility of individuals are denoted by $\alpha(x)$, $\beta(x)$, and $\nu(x)$, respectively. We assume that those rates are piecewise constant with the values α_i, β_i, and ν_i on each piece, $x \in \Omega_i$. The degree of bias, $-1 \leq z_i \leq 1$, at each interface determines two probabilities, $(1 - z_i)/2$ and $(1 + z_i)/2$, of moving to the left and to the right at boundary i, respectively [5]. The IDE describes how the population evolves in discrete time and continuous space. It assumes that individuals first reproduce according to a growth function, F, then disperse according to a dispersal kernel, k. The spatial variable x represents the location of a disperser at the end of the dispersal phase, while y represents the location of a disperser at the beginning of the dispersal phase. Let $N_t(x)$ denote the population density at the beginning of the growth phase in year t, and $F(N_t(x), x)$ denote the (possibly piecewise) population density at the end of the growth phase in year t, with $F(0, y) = 0$. Let $k(x, y)$ denote the dispersal kernel where $\int_x^{x+\Delta x} k(x, y)dx$ is the probability that an individual from y moves to $[x, x + \Delta x)$. Let $\mathcal{A}$ be the operator that maps the population density from one generation to the next,

$$N_{t+1}(x) = \mathcal{A}[N_t](x), \tag{2.1}$$

where

$$\mathcal{A}[N_t](x) = \int_\Omega k(x, y)F(N_t(y), y)dy. \tag{2.2}$$

We also assume that the linear operator $\mathcal{B}$ defined as

$$\mathcal{B}[N_t](x) = \int_\Omega k(x,y)R(y)N_t(y)dy, \tag{2.3}$$

is the linearization of $\mathcal{A}$ where $R(y) = \dfrac{d}{dN}F(N^*(y), y)$, in which N^* is a the trivial equilibrium of (2.2).

To investigate the long-term behaviour of the population, we make the following assumptions.

- The function k is a bounded non-negative function on $\Omega \times \Omega$, continuous within each patch, but with some possible discontinuities at patch boundaries a_i, where $i \in \{0, \ldots, 4\}$.
- The reproduction function F is non-negative, bounded above, increasing, and continuous on $[0, \infty)$.
- F is differentiable at 0 and $\frac{\partial}{\partial N}F(0,x) > 1$.
- The function F satisfies $\frac{F(u,x)}{u} < \frac{F(v,x)}{v}$, for all $u > v > 0$.

There exists a positive real principal eigenvalue, λ, of $\mathcal{B}$, and a nonzero eigenfunction, ϕ, of $\mathcal{B}$ such that $\mathcal{B}\phi = \lambda\phi$ [7]. The population will eventually undergo extinction, whenever $\lambda < 1$. Furthermore, the threshold $\lambda = 1$ is sharp in the sense that the population settles at a positive steady-state when $\lambda > 1$.

The equation $\mathcal{B}\phi = \lambda\phi$ implies that

$$\phi(x) = \frac{1}{\lambda} \sum_{j \in \{1,3\}} \int_{\Omega_j} R_j k(x,y)\phi(y)dy \quad x \in \Omega_i, i \in \{1,3\} \tag{2.4}$$

The sum is restricted to 1 and 3 because $R_0 = R_2 = R_4 = 0$, in which $R_j = F'(0,y)$ with $y \in \Omega_j$.

The dispersal kernel $k(x, y)$ is the Green's function of the operator

$$\mathcal{L} = \frac{\nu}{\alpha}\frac{\partial^2}{\partial x^2} - \frac{\alpha+\beta}{\alpha}, \tag{2.5}$$

with the following conditions.

$$k(y^-, y) = k(y^+, y), \tag{2.6}$$

$$k_x(y^-, y) - k_x(y^+, y) = \alpha_j/\nu_j, \tag{2.7}$$

$$\frac{\nu_i}{\alpha_i}(1+z_i)k(a_i^-, y) = \frac{\nu_{i+1}}{\alpha_{i+1}}(1-z_i)k(a_i^+, y), \tag{2.8}$$

$$\frac{\nu_i}{\alpha_i}k_x(a_i^-, y) = \frac{\nu_{i+1}}{\alpha_{i+1}}k_x(a_i^+, y), \tag{2.9}$$

where $i \in \{0, \ldots, 3\}$, $j \in \{0, \ldots, 4\}$, and $y \in \Omega_j$ [19] . The superscripts $-$ and $+$ are used to denote the left and right limits, respectively.

Applying the differential operator $\mathcal{L}$ to both sides of (2.4) implies that

$$\mathcal{L}\phi(x) = \frac{1}{\lambda}\sum_{j\in\{1,3\}}\int_{\Omega_j} R_j \mathcal{L}k(x, y)\phi(y)dy, \quad x \in \Omega_i, i \in \{1, 3\}, \tag{2.10}$$

$$\mathcal{L}\phi(x) = -\frac{1}{\lambda}\sum_{j\in\{1,3\}}\int_{\Omega_j} R_j \delta(x-y)\phi(y)dy, \quad x \in \Omega_i, i \in \{1, 3\}, \tag{2.11}$$

or

$$\mathcal{L}\phi(x) = -\frac{1}{\lambda}R_i\phi(x), \quad x \in \Omega_i, i \in \{1, 3\}. \tag{2.12}$$

Hence, within each patch, ϕ satisfies the following differential equation

$$\frac{\nu_i}{\alpha_i}\phi''(x) + \left(\tfrac{1}{\lambda}R_i - \frac{\alpha_i+\beta_i}{\alpha_i}\right)\phi(x) = 0, \quad x \in \Omega_i, i \in \{0, \ldots, 4\}. \tag{2.13}$$

Let $\phi_i(x)$ be the restriction of ϕ to Ω_i. Therefore, $\phi_i(x), i \in \Omega_i$, satisfies the following

differential equation.

$$\begin{aligned} &\phi_i''(x) - \mu_i^2 \phi_i(x) = 0, \qquad i \in \{0, 2, 4\} \\ &\phi_i''(x) + (\frac{\alpha_i}{\lambda \nu_i} R_i - \mu_i^2)\phi_i(x) = 0, \qquad i \in \{1, 3\} \end{aligned} \tag{2.14}$$

where $\mu_i = \sqrt{\dfrac{\alpha_i + \beta_i}{\nu_i}}$ denotes the decay rate of the dispersal.
Conditions (2.6) imply that ϕ_i satisfies the following boundary conditions.

$$\begin{aligned} \nu_0\alpha_1(1+z_0)\phi_0(a_0^-) &= \nu_1\alpha_0(1-z_0)\phi_1(a_0^+) \\ \nu_0\alpha_1\phi_0'(a_0^-) &= \nu_1\alpha_0\phi_1'(a_0^+) \\ \nu_1\alpha_2(1+z_1)\phi_1(a_1^-) &= \nu_2\alpha_1(1-z_1)\phi_2(a_1^+) \\ \nu_1\alpha_2\phi_1'(a_1^-) &= \nu_2\alpha_1\phi_2'(a_1^+) \\ \nu_2\alpha_3(1+z_2)\phi_2(a_2^-) &= \nu_3\alpha_2(1-z_2)\phi_3(a_2^+) \\ \nu_2\alpha_3\phi_2'(a_2^-) &= \nu_3\alpha_2\phi_3'(a_2^+) \\ \nu_3\alpha_4(1+z_3)\phi_3(a_3^-) &= \nu_4\alpha_3(1-z_3)\phi_4(a_3^+) \\ \nu_3\alpha_4\phi_3'(a_3^-) &= \nu_4\alpha_3\phi_4'(a_3^+) \end{aligned} \tag{2.15}$$

Moreover, $\phi(x) \to 0$ as $x \to \pm\infty$.
Assuming $\frac{1}{\lambda}R_i - \frac{\alpha_i+\beta_i}{\alpha_i} > 0$, equation (2.14) together with (2.15) has a solution of the form

$$\begin{aligned} \phi_0(x) &= A_0 e^{\mu_0 x} \\ \phi_1(x) &= A_1 \sin\omega_1 x + B_1 \cos\omega_1 x \\ \phi_2(x) &= A_2 e^{\mu_2 x} + B_2 e^{-\mu_2 x} \\ \phi_3(x) &= A_3 \sin\omega_3 x + B_3 \cos\omega_3 x \\ \phi_4(x) &= B_4 e^{-\mu_4 x} \end{aligned} \tag{2.16}$$

where A_i's and B_j's can be determined from the boundary conditions (2.15), and

$$\omega_i^2 = \frac{\alpha_i}{\lambda\nu_i}R_i - \frac{\alpha_i + \beta_i}{\nu_i}, \qquad i \in \{1, 3\}. \tag{2.17}$$

2.3 Gap-size calculation

To find an implicit function that describes the relation between the gap-size, l, the total length of the reserve area, L, and the other parameters defined in the previous section, we substitute (2.16) into (2.6). This gives us a homogeneous matrix equation

$$\mathbf{MX} = \mathbf{O}, \tag{2.18}$$

where $\mathbf{X}$ represents a vector that consists of the 8 coefficients, which are arranged in the same order as they appear in (2.16). Furthermore, $\mathbf{M}$ denotes a matrix whose elements are functions of L, l, and other parameters to the problem.

The boundary condition problem (2.14) with (2.6) has a non-trivial solution if

$$det(\mathbf{M}) = 0. \tag{2.19}$$

Since we assume that the boundaries at a_0 and a_3 are impermeable, meaning that no individual can cross them or leave the region, we have $z_0 = 1$ and $z_3 = -1$. This means $A_0 = B_4 = 0$. We do not need to know the exact values of the other coefficients, but we can simplify (2.19) to get the desired implicit function.

After setting $z_0 = 1$ and $z_3 = -1$, (2.19) implies that

$$\begin{aligned}
&\mathcal{P}\sinh(\mu_2 l)\Big[\epsilon_2 \sin\omega_3(\frac{L-l}{2})\sin\omega_1(\frac{L-l}{2}) + \epsilon_3\cos\omega_3(\frac{L-l}{2})\cos\omega_1(\frac{L-l}{2})\Big] \\
&= \mathcal{P}\cosh(\mu_2 l)\Big[\epsilon_1 \sin\omega_3(\frac{L-l}{2})\cos\omega_1(\frac{L-l}{2}) + \epsilon_4\cos\omega_3(\frac{L-l}{2})\sin\omega_1(\frac{L-l}{2})\Big]
\end{aligned} \tag{2.20}$$

where

$$\mathcal{P} = 2\alpha_0\alpha_1\alpha_2^2\alpha_3\alpha_4\nu_1^3\nu_2^4\nu_3^3\omega_1\omega_3(1-z_1)(1-z_2) \tag{2.21}$$

and

$$\begin{aligned}
\epsilon_1 &= \mu_2\omega_3(\tfrac{1+z_1}{1-z_1})(\tfrac{1+z_2}{1-z_2}) \\
\epsilon_2 &= \omega_1\omega_3(\tfrac{1+z_2}{1-z_2}) \\
\epsilon_3 &= \mu_2^2(\tfrac{1+z_1}{1-z_1}) \\
\epsilon_4 &= \mu_2\omega_1
\end{aligned} \tag{2.22}$$

If individuals do not bias their movement at the fishing zone boundaries, then

$$z_1 = z_2 = 0. \tag{2.23}$$

Also, assuming that the demography and dispersal parameters on either sides of the fishing zone are identical,

$$\begin{aligned}
\alpha_1 &= \alpha_3 \\
\beta_1 &= \beta_3 \\
\nu_1 &= \nu_3 \\
R_1 &= R_3,
\end{aligned} \tag{2.24}$$

hereafter we drop the subscripts when $i \in \{1, 3\}$.

The above set of assumptions simplifies (2.20) to

$$\frac{\sinh(\mu_2 l)}{\cosh(\mu_2 l)} = \frac{2\mu_2\omega\sin\omega(\frac{L-l}{2})\cos\omega(\frac{L-l}{2})}{\omega^2\sin^2\omega(\frac{L-l}{2}) + \mu_2^2\cos^2\omega(\frac{L-l}{2})}, \tag{2.25}$$

or

$$e^{2\mu_2 l} = \frac{\omega^2 \sin^2 \omega(\frac{L-l}{2}) + \mu_2^2 \cos^2 \omega(\frac{L-l}{2}) + 2\mu_2\omega \sin \omega(\frac{L-l}{2}) \cos \omega(\frac{L-l}{2})}{\omega^2 \sin^2 \omega(\frac{L-l}{2}) + \mu_2^2 \cos^2 \omega(\frac{L-l}{2}) - 2\mu_2\omega \sin \omega(\frac{L-l}{2}) \cos \omega(\frac{L-l}{2})}. \tag{2.26}$$

Let P denote the set of all parameters upon which the gap-size function depends. We can then define the implicit gap-size function as $G(l, \omega; P) = 0$, upon taking the square root of equation (2.26) as follows.

$$G(l, \omega; P) = e^{\mu_2 l} + \frac{1 + \frac{\omega}{\mu_2} \tan \omega(\frac{L-l}{2})}{1 - \frac{\omega}{\mu_2} \tan \omega(\frac{L-l}{2})} \tag{2.27}$$

2.4 Qualitative behavior of $G(l, \omega; P) = 0$ for selected parameter values

The non-zero steady-state is stable as long as the principal eigenvalue is greater than $\lambda = 1$, (Figure 2.2). Therefore, the critical gap-size $l^* = 4.6$ is obtained by solving the equation $G(l, \omega; P) = 0$ for l when $\lambda = 1$. If the gap-size exceeds this threshold, the species population in the protected area of length $L = 6$ will become extinct for the parameter values considered in this study.

According to the formula $\mu_2^2 = \frac{\alpha_2 + \beta_2}{\nu_2}$, μ_2 increases when either the settling rate, α_2 in the fishing zone increases, or when the motility, ν_2, in the fishing zone decreases. A higher μ_2 implies a lower l^* to ensure the persistence of the population for the parameter values considered in this study (Figure 2.3). This means that when individuals are more likely to settle in the fishing zone, or when they move slower in it and spend more time there, a shorter fishing area is needed to maintain the population in the lake.

A longer fishing zone requires a higher reproduction rate in the no-take area to

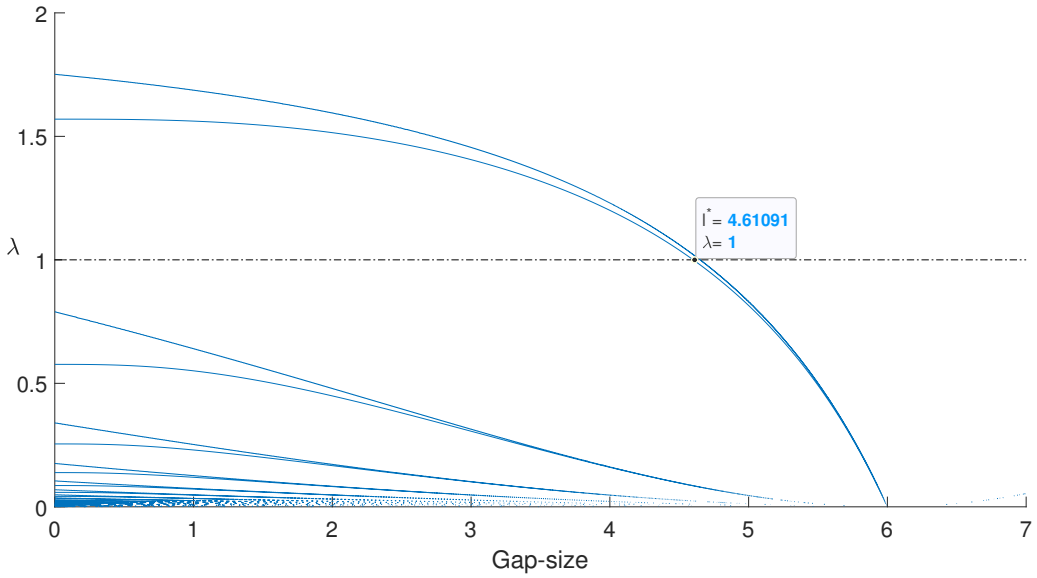

Figure 2.2: The plot illustrates the real eigenvalues of the equation (2.4) for different values of l, the length of the fishing zone, when $G(l, \omega; P) = 0$. The other parameters are fixed as follows: $L = 6, R = 2, \alpha = 2, \beta = 0, \nu = 2$, and $\mu_2 = 0.8$. In the figure, the critical gap-size, denoted as $l^* = 4.6$, is determined by setting the eigenvalue λ to 1 in the equation (2.17). Subsequently, the equation $G(l, \omega; P) = 0$ is solved for l to obtain this value.

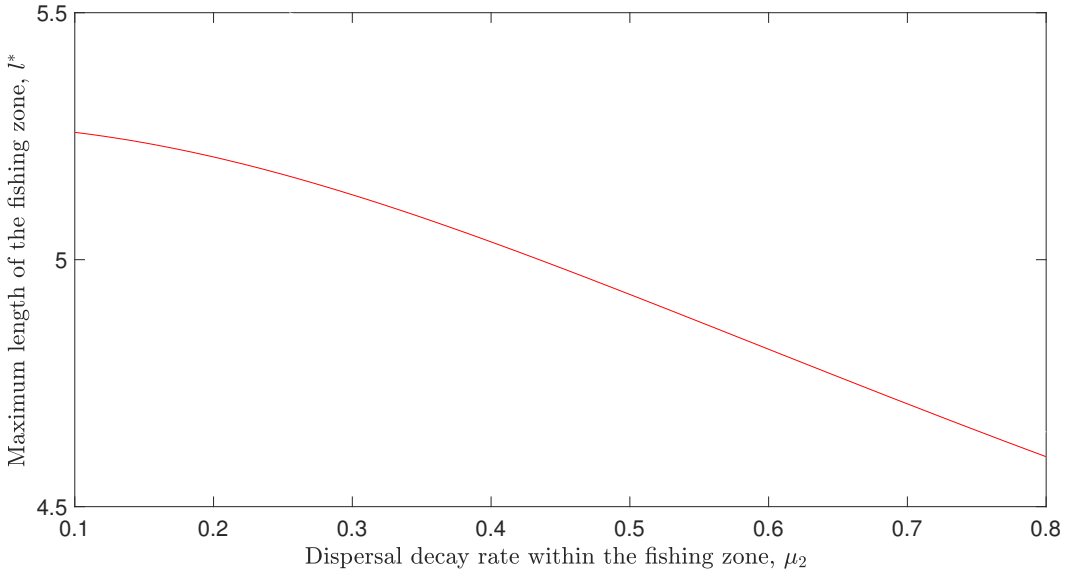

Figure 2.3: By setting the threshold eigenvalue λ to 1 in the equation $G(l, \omega; P) = 0$, we derive the maximum length of the fishing zone. This length is observed to be an inversely proportional of μ_2. This relationship holds when the other parameters are held constant at the following values: $L = 6, R = 2, \alpha = 2, \beta = 0, \nu = 2$.

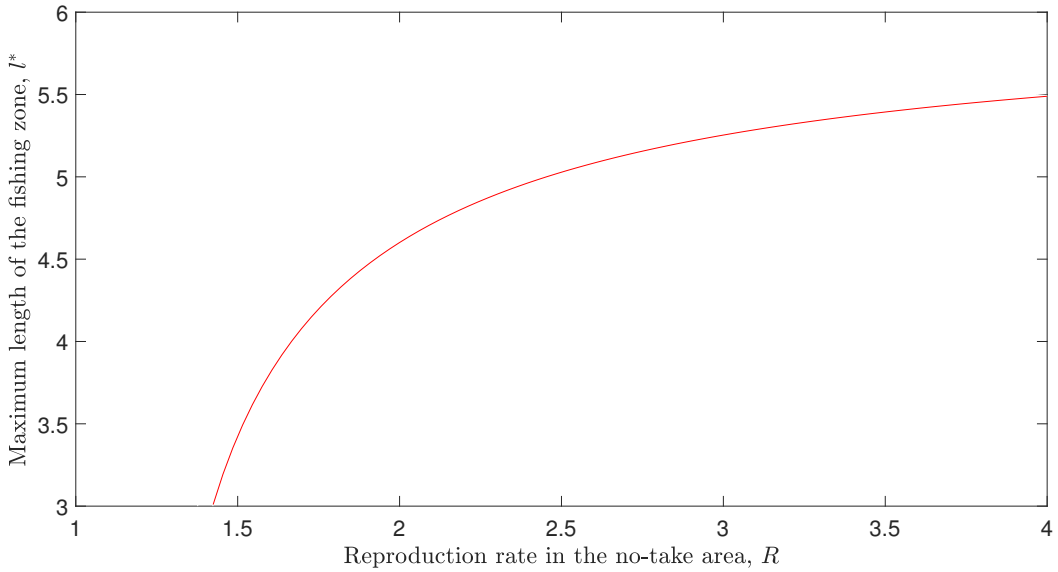

Figure 2.4: The curve illustrates an initial steep increase in l^* with a small increase in R, indicating a high sensitivity of the fishing zone to changes in the reproduction rate at low levels of R. As R continues to increase, the growth of l^* becomes more gradual, suggesting a diminishing return on the length of the fishing zone for higher reproduction rates. The concave downward shape of the curve further emphasizes this diminishing return effect. In the figure, the relationship between the maximum length of the fishing zone and the reproduction rate in the no-take zone, is generated by setting the threshold eigenvalue λ to 1 in the equation $G(l, \omega; P) = 0$, when the other parameters are held constant at the following values: $L = 6, \alpha = 2, \beta = 0, \nu = 2, \mu_2 = 0.8$.

sustain the total population in the lake (Figure 2.4). The no-take sides of the lake can support each other and prevent population collapse. Furthermore, increasing the gap between the no-take sides of the lake, but considering the upper limit $l^* < L$, does not lead to population extinction when the reproduction rate in the non-fishing parts of the lake is increased and high.

2.5 Discussion

We considered a habitat that is both closed and bounded with rigid boundaries, such as a lake, implying that no disperser can exit the habitat. This habitat serves as the one-dimensional domain for an Integro-Difference Equation (IDE). Our study focused

on the minimum requirements for persistence of the population, given the existence of a non-reproductive gap, such as fishing zone, at the center of the habitat. We developed an implicit function that is linked two key aspects: the demography and dispersal parameters of a species, and the total length of the non-reproductive gap. The eigenvalue problem corresponded to this scenario led us to the function. This new function established a relationship between the dominant eigenvalue and the maximum length of the gap beyond which the population would collapse. For selected parameter values, the qualitative behaviour of the implicit function illustrates how the optimal fishing zone length depends on the dispersal decay rate of the individuals. We found that when individuals are more likely to settle in the fishing zone, or when they move slower in it and spend more time there, the fishing area must be shorter, and the no-take length must be larger to maintain the population in the lake. On the other hand, the relationship between the maximum length of the fishing zone, l^*, and the reproduction rate in the no-take zone, R, illustrates an initial steep increase in l^* with a small increase in R, indicating a high sensitivity of the fishing zone to changes in the reproduction rate at low levels of R. As R continues to increase, the growth of l^* becomes more gradual, suggesting a diminishing return on the length of the fishing zone for higher reproduction rates.

In the process of formulating our mathematical model, we made an assumption that individuals' movements are not influenced by the boundaries of the fishing zones. This assumption simplified our formulation, resulting in a more compact version of the implicit function. However, future work could consider relaxing this assumption to account for the spillover effect. The spillover effect is a well-documented phenomenon in marine conservation, where fish and other marine species migrate from protected areas, or no-take zones, to adjacent areas open to fishing. This migration typically occurs when the population density in the no-take zone rises due to the absence of fishing pressure [18]. Consequently, certain individuals, especially those

nearing adulthood, may venture into the fishing zones.

Chapter 3

Critical patch size

The critical patch size refers to the smallest extent of a favorable area beneath which the population risks extinction. This study calculates the critical patch size, taking into account the demographic and dispersal traits of individuals, and acknowledges that these traits may vary across patches. Our findings indicate that the smallest critical patch size is attained when individuals have a tendency to leave the patch, enabling them to spread across two semi-infinite domains and potentially discover a suitable habitat. Conversely, the largest critical patch size is noted when the boundaries are more limiting, indicating a reduced probability of individuals leaving the patch. This situation reflects a real-world scenario where the enclosed patch essentially becomes the sole viable refuge for individuals to establish, adapt, and thrive.

As discussed in chapter 2, in a coastline segmented by a rock formation, a maximum gap size is expected to exist. Below this size, populations can thrive, but beyond it, they risk extinction. This threshold is called the critical separation length. Simulation results suggest that the critical separation length is minimized when the total habitat is divided into two equal parts. Our findings reveal that when the habitat is evenly split, neither side can independently maintain the minimum population

due to their diminished sizes. As a result, both segments become interdependent, requiring cooperation to ensure the survival and persistence of the entire population.

3.1 Introduction

The critical patch size, a key concept in spatial ecology, denotes the habitat size where population gains from reproduction offset losses from dispersal [11]. Initially, a truncated Laplace kernel into an IDE was introduced to compute the critical patch size based on the population's demography and dispersal traits in a single isolated patch [22]. The concept of a good-bad periodic domain was first proposed by Musgrave and Lutscher (2014) [15] for the Laplace kernel, extending the critical patch formula to scenarios where individuals exhibit biased movement at patch boundaries. The kernel was further expanded by introducing a multi-patch Laplace kernel, allowing for varying demography and dispersal traits across multiple patches [5]. This kernel facilitated the extension of the critical patch size formula to cases with varying degrees of bias at patch boundaries and differing characteristics from one patch to another.

A question in conservation ecology is how to calculate the smallest length of suitable habitat that can sustain a population over time. This question often arises when dealing with a species that lives in a limited, uniform patch of good habitat, surrounded by two large patches of poor habitat. Individuals dwelling near the boundaries are inclined to remain and reproduce within their existing habitat, rather than venturing into the surrounding patches [11]. In habitats that are one-dimensional, such as coastlines, individuals may bias their movement when they encounter the boundary between good and bad patches. However, we cannot assume that the same adjustment happens at both boundaries. The bias in movement may differ depending on whether the individual is moving from the left or the right side of the patch.

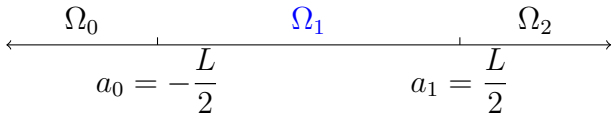

Figure 3.1: In a one-dimensional space, a favorable patch, Ω_1 is surrounded by two semi-infinite unfavorable patches Ω_0 and Ω_2

Previous studies have investigated the scenario where a favorable habitat is bounded by semi-infinite unfavorable regions, and have assumed that the bias level is identical at both boundary points. Moreover, it was assumed that the individuals have the same demographic and dispersal characteristics in both unfavorable regions [14]. We obtain an expression to compute the critical patch size based on the demographic and dispersal characteristics of the individuals, allowing for the possibility that these characteristics may differ among patches, regardless of whether they are favorable or unfavorable. The critical patch size expression will give the minimum length of the favorable region, below which the population will go extinct.

3.2 Notations and mathematical formulations

The whole real line is considered as the domain, Ω, and is divided into three sub intervals, Ω_j, for $j \in \{0, 1, 2\}$, as shown in Figure 3.1, by assuming that Ω_1 is the favorable patch. For each patch Ω_i, similar to the section 2.2, the settling rate, the death rate, and the motility of individuals are denoted by α_i, β_i, and ν_i, respectively. The degree of bias, $-1 \leq z_i \leq 1$, at each interface determines two probabilities, $(1 - z_i)/2$ and $(1 + z_i)/2$, of moving to the left and to the right at boundary i, respectively. The population we consider has a life cycle that can be modeled by an integrodifference equation (IDE) as discussed in section 2.2.

Van Kirk and Lewis (1997) [22] showed that the stability of the non-trivial solution to equation (2.2) gives rise to the eigenvalue problem 2.3, $\lambda\phi(x) = \mathcal{B}[\phi(x)]$, which

can be equivalently expressed as

$$\phi(x) = \frac{1}{\lambda} \sum_{j=0}^{2} \int_{\Omega_j} R_j k(x,y)\phi(y)dy, \quad x \in \Omega_i, i \in \{0,1,2\}. \tag{3.1}$$

By applying the differential operator $\mathcal{L}$ in 2.5 to both sides of equation (3.1), we obtain

$$\mathcal{L}\phi(x) = -\frac{1}{\lambda} R_i \phi(x), \quad x \in \Omega_i, i \in \{0,1,2\}. \tag{3.2}$$

This implies that within each patch, ϕ satisfies the differential equation

$$\frac{\nu_i}{\alpha_i}\phi''(x) + \left(\tfrac{1}{\lambda}R_i - \frac{\alpha_i + \beta_i}{\alpha_i}\right)\phi(x) = 0, \quad x \in \Omega_i, i \in \{0,1,2\}. \tag{3.3}$$

The interface conditions, as outlined in [15], are given by

$$\nu_i \alpha_{i+1}(1+z_i)\phi(a_i^-) = \nu_{i+1}\alpha_i(1-z_i)\phi(a_i^+),$$
$$\nu_i \alpha_{i+1}\phi_x(a_i^-, y) = \nu_{i+1}\alpha_i\phi_x(a_i^+, y).$$

Lastly, it is important to note that $\phi(x)$ approaches zero as x tends towards positive or negative infinity.

We assume that in both unfavorable patches no reproduction happens, that is $R_0 = R_2 = 0$. Therefore, we have the boundary value problem

$$\phi''(x) - \frac{\alpha_i + \beta_i}{\nu_i}\phi(x) = 0, \quad x \in \Omega_i, i \in \{0,2\}, \tag{3.4}$$
$$\phi''(x) + \left(\frac{\alpha_1 R_1}{\lambda \nu_1} - \frac{\alpha_1 + \beta_1}{\nu_1}\right)\phi(x) = 0, \quad x \in \Omega_1. \tag{3.5}$$

along with the four interface conditions and two limits at infinity,

$$\nu_0\alpha_1(1+z_0)\phi(a_0^-) = \nu_1\alpha_0(1-z_0)\phi(a_0^+)$$
$$\nu_0\alpha_1\phi'(a_0^-) = \nu_1\alpha_0\phi'(a_0^+)$$
$$\nu_1\alpha_2(1+z_1)\phi(a_1^-) = \nu_2\alpha_1(1-z_1)\phi(a_1^+)$$
$$\nu_1\alpha_2\phi'(a_1^-) = \nu_2\alpha_1\phi'(a_1^+).$$

Solving the boundary value problem outside the patch leads to

$$\phi(x) = A_0\exp(\mu_0 x), \quad x < -L/2,$$
$$\phi(x) = A_2\exp(-\mu_2 x), \quad x > L/2.$$

Hence, we can cast the eigenvalue problem as a boundary value problem on the interval $(-L/2, L/2)$.

$$\phi''(x) + \left(\frac{\alpha_1 R_1}{\lambda\nu_1} - \frac{\alpha_1+\beta_1}{\nu_1}\right)\phi(x) = 0, \quad -L/2 < x < L/2 \tag{3.6}$$
$$\nu_0\alpha_1(1+z_0)A_0\exp(-\mu_0 L/2) = \nu_1\alpha_0(1-z_0)\phi(-L/2) \tag{3.7}$$
$$\mu_0\nu_0\alpha_1 A_0\exp(-\mu_0 L/2) = \nu_1\alpha_0\phi'(-L/2) \tag{3.8}$$
$$\nu_1\alpha_2(1+z_1)\phi(L/2) = \nu_2\alpha_1(1-z_1)A_2\exp(-\mu_2 L/2) \tag{3.9}$$
$$\nu_1\alpha_2\phi'(L/2) = -\nu_2\alpha_1\mu_2 A_2\exp(-\mu_2 L/2) \tag{3.10}$$

Eliminating $\exp(-\mu_0 L/2)$ from (3.7) and (3.8) and eliminating $\exp(-\mu_2 L/2)$ from (3.9) and (3.10) give us

$$\mu_0(1-z_0)\phi(-L/2) - (1+z_0)\phi'(-L/2) = 0, \tag{3.11}$$
$$\mu_2(1+z_1)\phi(L/2) + (1-z_1)\phi'(L/2) = 0. \tag{3.12}$$

Now, we set $\tau_0 = \frac{\mu_0(1-z_0)}{1+z_0}$ and $\tau_2 = \frac{\mu_2(1+z_1)}{1-z_1}$ to obtain

$$\tau_0\phi(-L/2) - \phi'(-L/2) = 0, \tag{3.13}$$

$$\tau_2\phi(L/2) + \phi'(L/2) = 0. \tag{3.14}$$

Despite the exponential solution provided by Equation (3.4), Equation (3.5) may yield a solution in various forms: exponential, trigonometric, or even linear. This behavior depends on the sign of the expression $\left(\frac{\alpha_1 R_1}{\lambda\nu_1} - \frac{\alpha_1+\beta_1}{\nu_1}\right)$.
To explore this further, we consider three distinct cases in Equation (3.6). However, our analysis reveals that only one of these cases is feasible:

1. If $\lambda > \frac{\alpha_1 R_1}{\alpha_1+\beta_1}$,
2. If $\lambda = \frac{\alpha_1 R_1}{\alpha_1+\beta_1}$,
3. If $\lambda < \frac{\alpha_1 R_1}{\alpha_1+\beta_1}$.

In each scenario, we investigate whether the largest positive eigenvalue exists.

3.2.0.1 Case 1, $\lambda > \frac{\alpha_1 R_1}{\alpha_1+\beta_1}$

In this case, $\frac{\alpha_1+\beta_1}{\nu_1} - \frac{\alpha_1 R_1}{\lambda\nu_1} > 0$. So we define ω as

$$\omega = \sqrt{\frac{\alpha_1+\beta_1}{\nu_1} - \frac{\alpha_1 R_1}{\lambda\nu_1}}. \tag{3.15}$$

The solutions of the boundary problem are

$$\phi(x) = A\sinh\omega x + B\cosh\omega x$$

where A and B must satisfy

$$\tau_0(-A\sinh\omega L/2 + B\cosh\omega L/2) - (A\omega\cosh\omega L/2 - B\omega\sinh\omega L/2) = 0, \quad (3.16)$$

$$\tau_2(A\sinh\omega L/2 + B\cosh\omega L/2) + (A\omega\cosh\omega L/2 + B\omega\sinh\omega L/2) = 0. \quad (3.17)$$

Equations (3.16) and (3.17) are linear and homogeneous, so there are non zero solutions A and B if and only if the determinant is zero, which implies that

$$\big(\tau_0\tau_2 + \omega^2\big)\sinh(\omega L) = -\omega\big(\tau_0 + \tau_2\big)\cosh(\omega L). \quad (3.18)$$

Therefore, to find the dominant eigenvalue, we need to find the largest value of ω, (see 3.15), which satisfies the equation

$$\tanh(\omega L) = \frac{-\omega(\tau_0 + \tau_2)}{\tau_0\tau_2 + \omega^2}. \quad (3.19)$$

The left side is strictly increasing and zero for $\omega = 0$, and the right side is negative for all positive omega. That is, in this case the the equation has no positive solutions.

3.2.0.2 Case 2, $\lambda = \frac{\alpha_1 R_1}{\alpha_1+\beta_1}$

In this case also there is no eigenvalue for the model. In fact, under the assumption of this case, Equation (3.6) has a solution of the form

$$\phi(x) = Ax + B.$$

Eliminating B/A in (3.13) and (3.14) leads to

$$(\tau_0 + \tau_2) + \tau_0\tau_2 L = 0,$$

which has contradiction with positivity of τ_0, τ_2 and L.

3.2.0.3 Case 3, $\lambda < \frac{\alpha_1 R_1}{\alpha_1+\beta_1}$

In this case, $\frac{\alpha_1 R_1}{\lambda\nu_1} - \frac{\alpha_1+\beta_1}{\nu_1} > 0$. So we define ω as

$$\omega^2 = \frac{\alpha_1 R_1}{\lambda\nu_1} - \frac{\alpha_1+\beta_1}{\nu_1}. \tag{3.20}$$

The solutions of the boundary problem are

$$\phi(x) = A\sin\omega x + B\cos\omega x,$$

where A and B must satisfy

$$-\tau_0 \sin\omega L/2 + \tau_0(B/A)\cos\omega L/2 - \omega\cos\omega L/2 - (B/A)\omega\sin\omega L/2 = 0, \tag{3.21}$$

$$\tau_2 \sin\omega L/2 + \tau_2(B/A)\cos\omega L/2 + \omega\cos\omega L/2 - (B/A)\omega\sin\omega L/2 = 0. \tag{3.22}$$

Equations (3.21) and (3.22) are linear and homogeneous, so there are non zero solutions A and B if and only if the determinant is zero, which implies that

$$\big(\omega^2 - \tau_0\tau_2\big)\sin(\omega L) = \omega\big(\tau_0+\tau_2\big)\cos(\omega L). \tag{3.23}$$

In order to find the dominant eigenvalue, we need to find the smallest positive value of ω, (see 3.20), which satisfies the equation

$$\tan(\omega L) = \frac{\omega(\tau_0+\tau_2)}{\omega^2 - \tau_0\tau_2}. \tag{3.24}$$

The trivial equilibrium loses its stability when the dominant eigenvalue passes through the unit circle. Therefore, setting the threshold $\lambda = 1$ in (3.20)

$$\omega_1^2 = \frac{\alpha_1 R_1}{\nu_1} - \frac{\alpha_1+\beta_1}{\nu_1}, \tag{3.25}$$

turns Equation (3.24) to a formula to calculate the critical domain length L^*,

$$L^* = \frac{1}{\omega_1} \tan^{-1}\Big(\frac{(\tau_0+\tau_2)\omega_1}{\omega_1^2 - \tau_0\tau_2}\Big). \tag{3.26}$$

3.3 Qualitative behavior of the critical patch size

Equation (3.26) delineates the correlation between the critical domain length and the intrinsic growth rate at the bifurcation point. This equation provides a direct method to ascertain the critical patch size in a scenario where a single isolated patch is encircled by two semi-infinite unfavorable patches with no chance of reproduction, each potentially exhibiting a different boundary bias. The critical patch size is expressed as a function of τ_0, ω_1, and τ_2, which denote the habitat quality in patches Ω_0, Ω_1, and Ω_2, respectively, in addition to the degree of bias at the patch boundaries. The Equation (3.26) gives a positive value for L^*, if

$$\omega_1^2 > \tau_0\tau_2. \tag{3.27}$$

The maximum critical patch size corresponds to the highest positive values of z_1 and the most negative values of z_0, (Figure 3.2). A positive $z_i, i \in \{0,1\}$ indicates a bias in the dispersers' movement to the right of $a_i, i \in \{0,1\}$, while a negative z_i suggests the opposite. When individuals are inclined to leave the patch (signified by a highly positive z_0 and a highly negative z_1), the smallest value of L^* is observed. This is because the individuals have the opportunity to disperse across two semi-infinite domains, potentially finding a suitable habitat. Conversely, when the boundaries become more restrictive, implying a low probability of leaving the patch (a highly negative z_0 and a highly positive z_1), the maximum value of L^* is observed. This reflects the reality that the enclosed patch is virtually the only available habitat for individuals to establish and survive.

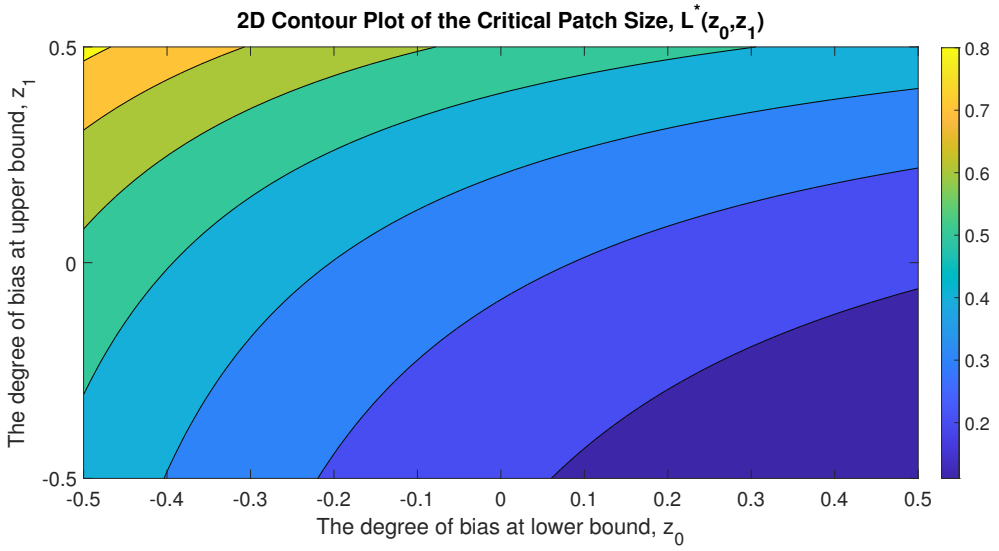

Figure 3.2: This plot illustrates the critical patch size, L^*, as determined by equation (3.26). It is depicted as a function of the degrees of bias, z_0 and z_1, at the interval bounds a_0 and a_1. The parameters in equation (3.26) are held constant: $\mu_0 = \mu_2 = 0.5, \alpha_1 = 2, \beta_1 = 0, \nu_1 = 2, R_1 = 4$. The contour is plotted by assuming $-0.5 \leq z_{0,1} \leq 0.5$, however it can be extended to $-1 \leq z_{0,1} \leq 1$ as long as the condition (3.27) is met. The point $(0, 0)$ on the plot corresponds to the critical patch size calculated in [22] for an isolated patch with no movement bias ($z_0 = z_1 = 0$) at the boundaries. Points on $z_1 = |z_0|$ represent the critical patch sizes calculated in [14] under the condition of identical boundary biases, given $\mu_2 = \mu_0$.

When there is no bias at boundaries and the habitat quality is the same in Ω_0 and Ω_2, then the inequality (3.27) turns to

$$\mu_0^2 + \mu_1^2 < \frac{\alpha_1}{\nu_1} R_1, \tag{3.28}$$

which is another criteria for the existence of the non-trivial equilibrium. In a very special case in which the death rate during the dispersal phase is zero, the necessary condition for the existence of the non-trivial solution becomes

$$\frac{\alpha_1}{\nu_1}(R_1 - 1) > \frac{\alpha_0}{\nu_0}. \tag{3.29}$$

Inequality (3.29) is in agreement with the case that the landscape is homogeneous and the growth rate R_1 has to satisfy $R_1 > 1$.

3.4 Supporting patches

In scenarios where a single patch exceeding the critical length is divided into two smaller patches by an intervening unfavorable patch, numerous intriguing questions about persistence emerge. Consider, for instance, a coastline interrupted by a rock formation. It is anticipated that there exists a maximum gap size, below which populations continue to thrive, and beyond which they cease to exist. This threshold is referred to as the critical separation length.

The critical separation length is dependent on the total length of the favorable patches. By incorporating the multi-patch Laplace kernel, initially derived by [4], into an Integral Differential Equation (IDE), we were able to simulate three distinct scenarios of the critical separation length. The critical separation length is an increasing function of $L = L_1 + L_2$, indicating that the populations on either side of the gap can mutually sustain as the gap size enlarges, provided the total length of

their habitat extends, (Figure 3.3). Three different proportions of the total length have been allocated to the first patch. For instance, in the simulation represented by the blue curve, $L_1 = aL$ and $L_2 = (1-a)L$, where $a = 0.2$ signifies the fraction of the first patch of the domain size. The pronounced leap in the graph possibly underscores the phenomenon that individuals initially disperse from the shorter segment and settle in the longer, and thus more favorable, part of the patch.

The results of the simulation indicate that the critical separation length reaches its minimum value when the total habitat is bifurcated into two equal segments. This is clearly illustrated by the green curve corresponding to the scenario where $a = 0.50$ (Figure 3.3). Upon comparing this curve with those representing other habitat division scenarios, it becomes evident that an equal division of the habitat does not provide sufficient size on either side to support the minimum length required for population persistence. This observation underscores the interdependence of the two sides in maintaining the overall population. In other words, when the habitat is equally partitioned, neither side can independently sustain the minimum population due to their reduced sizes. Consequently, both sides become mutually reliant, necessitating cooperation to ensure the survival and persistence of the entire population. This finding has significant implications for understanding population dynamics in fragmented habitats and could inform strategies for habitat management and conservation.

3.5 Discussion

The critical patch size formula derived earlier (Equation 3.26), indicates that the minimum critical patch size is achieved when individuals are predisposed to leave the patch, as they can disperse across two semi-infinite domains and potentially locate a suitable habitat. On the other hand, the maximum value of the critical patch size,

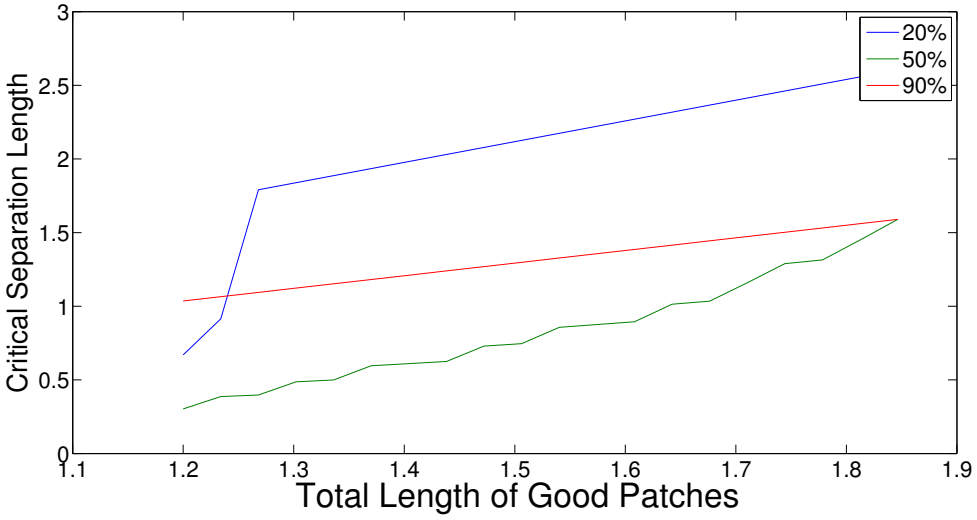

Figure 3.3: This plot presents the results of a numerical solution involving an Integro-Difference Equation (IDE) with a domain comprising two good patches separated by a bad patch. Each good patch constitutes a portion of the total length, and 20 test points are employed to simulate the relationship between the critical separation length and the total length of the good patches. The IDE in this simulation incorporates a Multi Patch Laplace kernel and a Beverton-Holt reproduction function, with parameters $\alpha = 3$, $\beta = 1$, and $\nu = 2$. It is noteworthy that the growth rate in the good patches is assumed to be $R_g = 3$, while in the bad patch, it is $R_b = 0$. The simulation reveals an overall increasing trend across all three scenarios of habitat division. Interestingly, when the habitat is equally divided into two parts, the critical separation length exhibits the lowest values. This suggests that neither side can independently support the population, thereby necessitating mutual reliance for the sustenance of the entire population.

L^*, is observed when the boundaries are more restrictive, signifying a lower likelihood of individuals exiting the patch. This scenario mirrors the real-world situation where the enclosed patch essentially becomes the sole viable habitat for individuals to settle and survive.

The concept of a Critical Separation Length can be further elucidated by considering the impact of habitat on insect movements. Research has shown that dispersal through unsuitable habitats can reduce gene flow and thus reproductive success [13]. In the context of a coastline interrupted by a rock formation, if the gap created by the rock formation exceeds the Critical Separation Length, it could act as an unsuitable habitat for the species. This could potentially hinder movement and gene flow, leading to a decline in the population. Therefore, understanding the Critical Separation Length is crucial for predicting and managing the persistence of populations in fragmented habitats.

In the course of our research, we conducted a series of simulations that revealed a consistent upward trend across all three scenarios of habitat fragmentation. This trend was observed regardless of the specific conditions or parameters of the division, underscoring the robustness of our findings.

A particularly intriguing observation emerged when the habitat was bisected into two equal parts. In this scenario, the critical separation length - a key metric in our study - consistently registered the lowest values. Upon closer examination, this phenomenon suggests that when a habitat is evenly split, neither of the resulting sections can independently sustain the population. This is a significant insight as it implies a degree of interdependence between the two halves. The survival and prosperity of the species in question appear to hinge on a mutual reliance between the two sections of the habitat.

In conclusion, our study introduces the concept of Critical Separation Length as a novel, insightful metric in the field of ecology. It provides a quantitative measure of

the impact of habitat division on species persistence, thereby offering a valuable tool for future research and conservation efforts.

Chapter 4

Dispersal redistribution approximation

This study introduces an approximation method that simplifies the calculation of the equilibrium population in relation to local growth dynamics and the dispersal redistribution function in a patchy landscape. We develop a form of the redistribution approximation for a piecewise continuous kernel and provide an estimate of the approximation error. The accuracy of the approximation improves as the movement bias (see [4]) at patch boundaries increases. Our estimate is influenced by the derivative of the growth term and the deviation of the equilibrium solution from its average across patches. The estimate is exact if the kernel is piecewise constant.

Our main results are as follows. First, we obtain an error estimate for the redistribution approximation in the case of a piecewise homogeneous habitat. The result depends on the derivative of the growth term and the deviation of the equilibrium solution from its patch-wise average. Second, we find that the estimate is exact if the kernel is piecewise constant. Finally, we find that the error decreases as the degree of movement bias increases, indicating that our approximation is more accurate for landscapes with high bias at patch boundaries.

4.1 Introduction

Patchy landscapes are spatially heterogeneous areas where individuals may encounter several habitat patches during their dispersal stage. At each interface point between good and bad patches, individuals can perceive the presence of both habitat types and bias their movement towards the preferred habitat, as discussed by Ovaskainen and Cornell [19]. In this chapter, we present an approximation method that enables straightforward calculation of the equilibrium population in relation to local growth dynamics and the dispersal redistribution function in patchy landscape. We derive a form of the redistribution approximation for a piecewise continuous kernel and estimate the error of the approximation. We then study the dependence of the error on the movement bias in the simple case of a single isolated patch.

The method we use to derive the approximation also provides a way to approximate the dominant eigenvalue and the corresponding eigenfunction of an integrodifference equation in a patchy domain where the kernel may have discontinuities at patch boundaries, such as the multi-patch Laplace kernel initially derived by Beykzadeh and Watmough [5]. Later, it was demonstrated that the linear integral operator corresponding to the integrodifference equation has a unique, real eigenvalue with a positive eigenfunction [7].

4.2 Derivation of the approximation

Integrodifference equations serve as a tool in modeling the life cycles of annual species, particularly those with distinct phases of reproduction and dispersal. Consider a finite, patchy habitat denoted by $\Omega = \bigcup_{j=1}^{m} \Omega_j$, where each Ω_j represents a closed and bounded interval. Let's define $N_t(y)$ as the spatial population density at a given point $y \in \Omega$ during generation t, specifically at the onset of the reproduction phase. If we assume F is defined by $F_j(N)$ for $y \in \Omega_j$, then $F_j(N_t(y))$ signifies the

population density following the growth stage. In the subsequent dispersal stage, each individual has the potential to relocate from their current position to a new one, based on a certain probability. The dispersal kernel $k(x, y)$ represents the probability density that an individual, starting its movement from y, will end up at $x \in \Omega$ after the dispersal stage. Consequently, the spatial density of the population satisfies the following integrodifference equation.

$$N_{t+1}(x) = \sum_{j=1}^{m} \int_{\Omega_j} k(x, y) F_j\big(N_t(y)\big) dy \tag{4.1}$$

Let $N^*(x)$ be the fixed point of (4.1). We have

$$N^*(x) = \sum_{j=1}^{m} \int_{\Omega_j} k(x, y) F_j\big(N^*(y)\big) dy. \tag{4.2}$$

The average value of the equilibrium is defined by

$$\bar{N_j} = \frac{1}{V_{\Omega_j}} \int_{\Omega_j} N_j^*(x) dx, \tag{4.3}$$

where V_{Ω_j} represents the length of Ω_j.

According to the Mean Value Theorem, for each $y \in \Omega$,

$$F_j(N^*(y)) = F_j(\bar{N_j}) + F_j'(\hat{N}_j(y))\big(N^*(y) - \bar{N_j}\big), \tag{4.4}$$

for some $\hat{N}_j(y)$ between $\bar{N_j}$ and $N^*(y)$. Substituting (4.4) into (4.2) implies

$$N^*(x) = \sum_{j=1}^{m} \int_{\Omega_j} k(x, y)\Big(F_j(\bar{N_j}) + F_j'(\hat{N}_j(y))\big(N^*(y) - \bar{N_j}\big)\Big) dy, \tag{4.5}$$

or

$$N^*(x) = \sum_{j=1}^{m} F_j(\bar{N}_j) \int_{\Omega_j} k(x,y)dy + \sum_{j=1}^{m} \int_{\Omega_j} k(x,y) F_j'(\hat{N}_j(y)) \big(N^*(y) - \bar{N}_j\big) dy. \quad (4.6)$$

The dispersal redistribution function is defined as follows [9].

$$u_j(x) = \int_{\Omega_j} k(x,y)dy \quad (4.7)$$

Substituting (4.7) into (4.6) we have

$$N^*(x) = \sum_{j=1}^{m} F_j(\bar{N}_j) u_j(x) + \sum_{j=1}^{m} \int_{\Omega_j} k(x,y) F_j'(\hat{N}_j(y)) \big(N^*(y) - \bar{N}_j\big) dy. \quad (4.8)$$

Therefore, the first order approximation of the equilibrium solution is

$$N^*(x) \approx \begin{bmatrix} u_1(x) & u_2(x) & \cdots & u_m(x) \end{bmatrix} \begin{bmatrix} F_1(\bar{N}_1) \\ F_2(\bar{N}_2) \\ \vdots \\ F_m(\bar{N}_m) \end{bmatrix}. \quad (4.9)$$

Integrating both side of (4.6) over Ω_i implies that

$$\int_{\Omega_i} N^*(x)dx = \int_{\Omega_i} \sum_{j=1}^{m} F_j(\bar{N}_j) u_j(x) dx + \int_{\Omega_i} \sum_{j=1}^{m} \int_{\Omega_j} k(x,y) F_j'(\hat{N}_j(y)) \big(N^*(y) - \bar{N}_j\big) dy dx \quad (4.10)$$

Since $\bar{N}_j = (1/V_{\Omega_j}) \int_{\Omega_j} N^*(x)dx$, then

$$V_{\Omega_i}\bar{N}_i = \sum_{j=1}^{m} F_j(\bar{N}_j) \int_{\Omega_i} u_j(x)dx + \sum_{j=1}^{m} \int_{\Omega_j}\int_{\Omega_i} k(x,y)F_j'(\hat{N}_j(y))\big(N_j^*(y) - \bar{N}_j\big)dxdy, \quad (4.11)$$

or

$$V_{\Omega_i}\bar{N}_i = \sum_{j=1}^{m} F_j(\bar{N}_j) \int_{\Omega_i} u_j(x)dx + R_{ij}. \quad (4.12)$$

Neglecting the remainder terms, R_{ij}, leads to the approximation

$$V_{\Omega_i}\bar{N}_i = \sum_{j=1}^{m} V_{\Omega_i} F_j(\bar{N}_j)U_{ij}, \quad (4.13)$$

where U_{ij} is the spatial average of the redistribution function and is defined by

$$U_{ij} = \frac{1}{V_{\Omega_i}} \int_{\Omega_i} u_j(x)dx. \quad (4.14)$$

System (4.13) has the following matrix form

$$\begin{bmatrix} \bar{N}_1 \\ \bar{N}_2 \\ \vdots \\ \bar{N}_m \end{bmatrix} = \begin{bmatrix} U_{11} & U_{12} & \cdots & U_{1m} \\ U_{21} & U_{22} & \cdots & U_{2m} \\ \vdots & \vdots & & \vdots \\ U_{m1} & U_{m2} & \cdots & U_{mm} \end{bmatrix} \begin{bmatrix} F_1(\bar{N}_1) \\ F_2(\bar{N}_2) \\ \vdots \\ F_m(\bar{N}_m) \end{bmatrix}. \quad (4.15)$$

We assume that the system has a positive solution as follows.

$$\bar{N}^a = \begin{bmatrix} \bar{N}_1^a \\ \bar{N}_2^a \\ \vdots \\ \bar{N}_m^a \end{bmatrix} \quad (4.16)$$

Applying (4.15) gives us the dispersal redistribution approximation (DRA) as follows.

$$N^* \approx \begin{bmatrix} u_1 & u_2 & \cdots & u_m \end{bmatrix} \begin{bmatrix} U_{11} & U_{12} & \cdots & U_{1m} \\ U_{21} & U_{22} & \cdots & U_{2m} \\ \vdots & \vdots & & \vdots \\ U_{m1} & U_{m2} & \cdots & U_{mm} \end{bmatrix}^{-1} \begin{bmatrix} \bar{N}_1^a \\ \bar{N}_2^a \\ \vdots \\ \bar{N}_m^a \end{bmatrix} \tag{4.17}$$

4.3 Error analysis

The error of the DRA is the difference between $N^*(x)$ and its approximation

$$N^a(x) = \sum_{j=1}^{m} F_j(\bar{N}_j^a) u_j(x). \tag{4.18}$$

The difference can be written as

$$\begin{aligned} |N^*(x) - N^a(x)| &= |\sum_{j=1}^{m} \big(F_j(\bar{N}_j) - F_j(\bar{N}_j^a)\big) u_j(x) \\ &\quad - \int_{\Omega_j} k(x,y) F_j'(\hat{N}_j(y)) \big(N^*(y) - \bar{N}_j\big) dy| \\ &\leq |\sum_{j=1}^{m} M_{(1,j)} \big(\bar{N}_j - \bar{N}_j^a\big) u_j(x)| + |\int_{\Omega_j} k(x,y) M_{(1,j)} M_{(2,j)} dy|, \end{aligned}$$

in which $M_{(1,j)}$ is the Lipschitz constant of F_j, and $M_{(2,j)}$ denotes the maximum difference between the equilibrium and its average in each patch Ω_j.

If we define

$$M_1 := \max\{M_{(1,j)}, M_{(1,j)} M_{(2,j)}\} \qquad 1 \leq j \leq m \tag{4.19}$$

then

$$|N^*(x) - N^a(x)| \leq M_1 \Big(|\sum_{j=1}^{m} \big(\bar{N}_j - \bar{N}_j^a\big) u_j(x)| + |\sum_{j=1}^{m} u_j(x)| \Big), \tag{4.20}$$

which represents an upper bound for the error, depends on the difference between the average value of the equilibrium and the solution of the system (4.15).

4.4 Example, a patchy landscape including three patches with movement bias at boundaries

Consider two good patches, Ω_1 and Ω_3, separated by a bad patch Ω_2. The degree of bias at each boundary is 0.7. The length of each patch Ω_j is represented by L_j, and the reproduction functions are given by

$$F_j(N) = \frac{R_j N}{1 + (R_j - 1)N}. \tag{4.21}$$

We approximate the non-trivial equilibrium solution to (4.1) using (4.17). The approximation is shown in Figures (4.1) and (4.2).

While the approximation appears reasonable, errors are more noticeable when the bias at interfaces is lower (see Figure (4.2)). The absolute value of the difference between approximation and the estimated equilibrium via iteration is plotted in Figure (4.3). For different values of z, the error decreases as bias increases as the plot shows.

4.5 Discussion

The study of species dispersal and reproduction in nature necessitates an understanding of the equilibrium population and its relationship with habitat parameters. The dispersal redistribution approximation provides an estimate of the steady-state population in a landscape composed of various patches, each with a movement bias at its boundaries. This approximation has been applied to IDEs with both Laplace and piecewise continuous dispersal kernels, yielding minimal error in both cases.

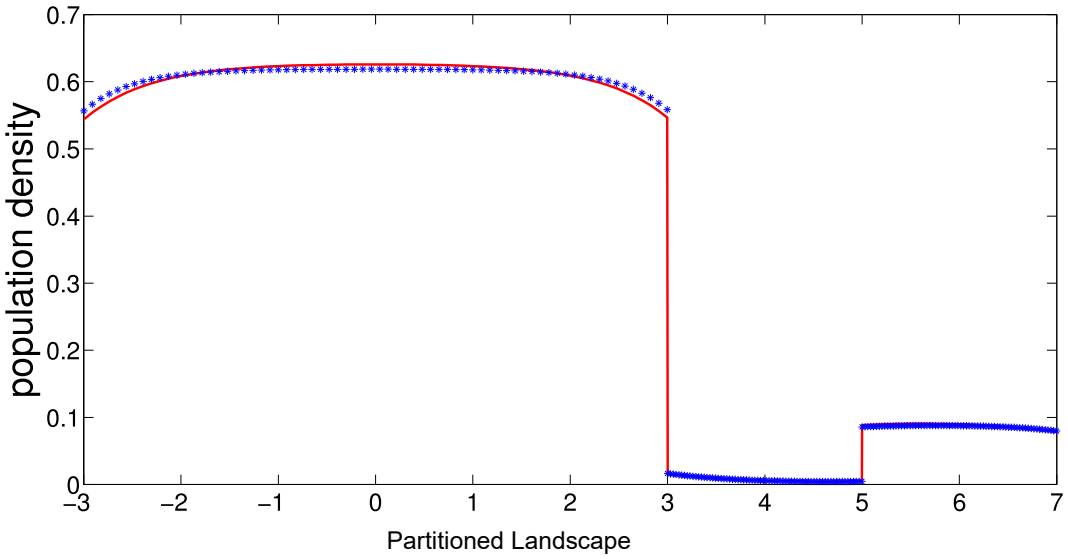

Figure 4.1: Approximation, in blue color, of dispersal distribution (4.17) in a landscape comprising three patches of varying habitat quality, with a higher bias at interfaces. Parameter are fixed as follows. Length of patches $|\Omega_1| = 6, |\Omega_2| = 2, |\Omega_3| = 2$. Settling rates, $\alpha_1 = 3, \alpha_2 = 1, \alpha_3 = 2$. Death rates $\beta_1 = 1, \beta_2 = 2, \beta_3 = 1.5$. Motilities $\nu_1 = 1, \nu_2 = 2, \nu_3 = 1.2$. Reproduction rates $R_1 = 3, R_2 = 0, R_3 = 2$. And finally the degree of bias at patch boundary between Ω_1 and Ω_2 equals -0.7, and at the interface point between Ω_2 and Ω_3 is 0.7.

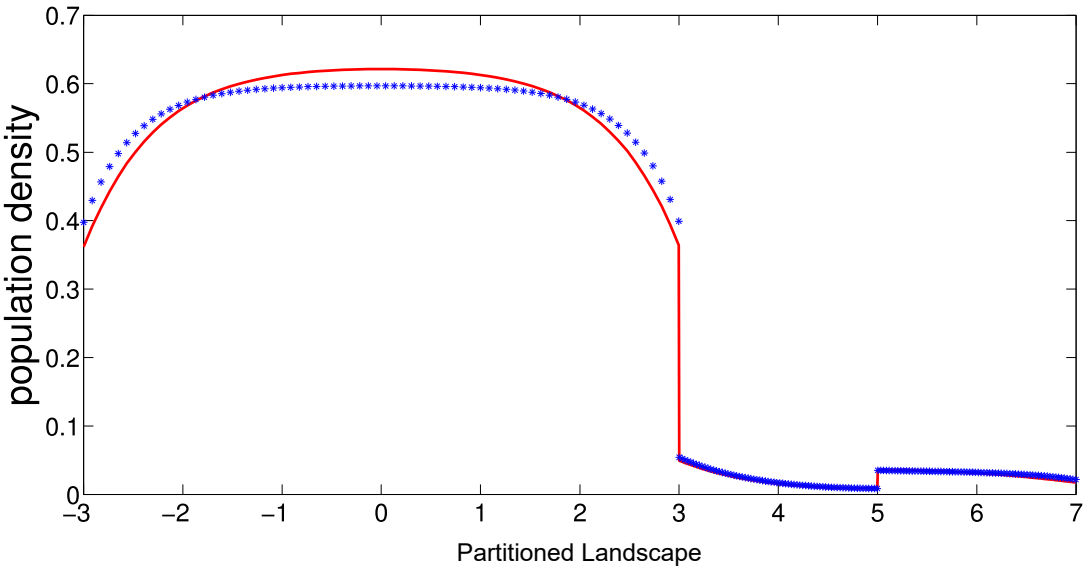

Figure 4.2: Approximation, in blue color, of dispersal distribution (4.17) in a landscape comprising three patches of varying habitat quality, with a lower bias at interfaces. The degree of bias at patch boundary between Ω_1 and Ω_2 equals -0.1, and at the interface point between Ω_2 and Ω_3 is 0.1. All other parameters are the same as Figure (4.1).

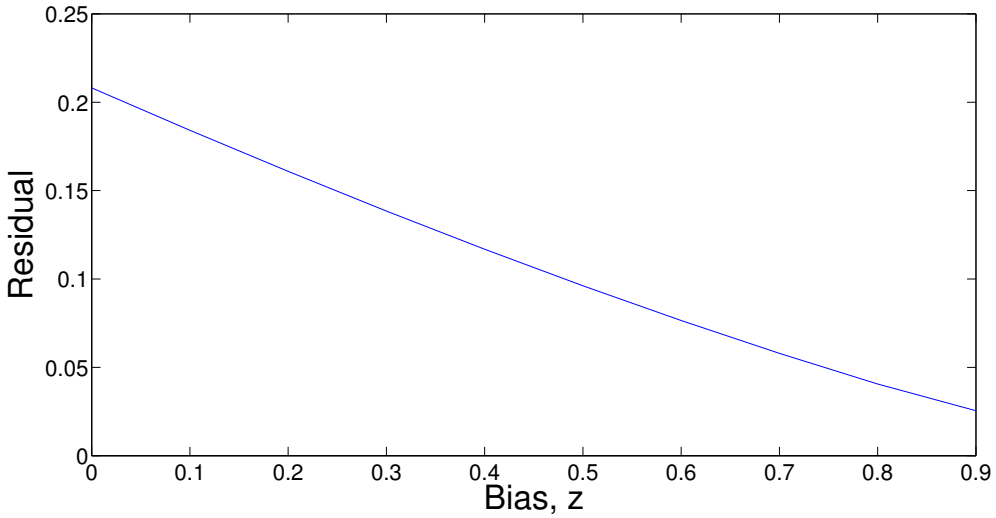

Figure 4.3: The norm of the difference between the approximation of the dispersal distribution and the true steady-state solution of the IDE decreases as a function of movement bias. The approximation is more accurate when the movement bias at patch boundaries is high.

In the context of patchy landscapes with bias at interfaces, which include connected homogeneous patches, these landscapes can be viewed as the domain of the dispersal kernel and the reproduction function in an IDE model. One of the key questions this raises is the impact of bias on the error of the dispersal redistribution approximation. There is an inverse relationship between the residual and the bias, a topic that warrants further investigation (Figure 4.3).

Broadly speaking, this research contributes to several larger questions.

1. How can we approximate the equilibrium distributions of populations inhabiting heterogeneous habitats? More specifically, we are interested in populations with distinct growth and dispersal stages, where the dynamics can be described by a dispersal kernel and a growth function, and where the heterogeneous habitat can be divided into patches with uniform characteristics for growth and dispersal.

2. What is the error analysis of the redistribution approximation?

Chapter 5

Discussions and Conclusions

In this chapter, we synthesize the findings from Chapters 2, 3, and 4, and discuss their implications for ecological theory and conservation practices. We reflect on the key insights gained from each study and propose avenues for future research in spatial ecology.

Chapter 2 delved into the persistence of populations inhabiting single isolated patches with hard boundaries. We discussed the implications of a non-reproductive gap, such as a fishing zone, within the habitat and explored the relationship between gap size and population persistence. Our findings shed light on the trade-offs involved in designing marine reserves and highlighted the importance of considering both demographic and dispersal parameters in conservation planning. Our research indicates that when individuals tend to settle within the fishing zone or move more slowly through it, necessitating longer stays, the fishing area should be smaller. On a different note, the relationship between the maximum length of the fishing zone, denoted as l^*, and the reproduction rate in the no-take zone, represented by R, exhibits an initial sharp increase in l^* with only a slight rise in R. This suggests that the fishing zone is highly sensitive to changes in the reproduction rate at lower levels of R. However, as R continues to increase, the growth of l^* becomes more gradual,

indicating diminishing returns on extending the fishing zone for higher reproduction rates.

Building upon the concept of critical patch size, Chapter 3 investigated the minimum habitat size required for population persistence in a landscape. By incorporating biased movement at patch boundaries, we extended previous models and derived a critical patch size formula applicable to diverse habitat configurations. Our analysis revealed the influence of habitat fragmentation on population dynamics and emphasized the need for tailored conservation strategies to mitigate the effects of habitat loss and degradation. We found that when individuals exhibit a tendency to leave the patch, the smallest value of the critical patch size is observed. This phenomenon occurs because these individuals have the opportunity to disperse across two semi-infinite domains, potentially discovering a suitable habitat. Conversely, as the boundaries become more restrictive, implying a low probability of leaving the patch, the maximum value of the critical patch size is observed. This reflects the reality that the enclosed patch serves as virtually the sole available habitat for individuals to establish and survive.

Chapter 4 focused on approximating the equilibrium population in a patchy landscape with varying habitat quality and biased dispersal. By developing a redistribution approximation method, we provided a framework for estimating population densities across multi-patch habitats. Our analysis demonstrated the utility of this approach in predicting population dynamics and assessing the impact of habitat structure on species persistence.

In conclusion, our approach has yielded valuable insights into the spatial dynamics of ecological systems. By integrating theoretical and experimental approaches, we can enhance our ability to predict and mitigate the impacts of habitat fragmentation on biodiversity. As we continue to refine our models and expand our empirical research, we remain committed to advancing the field of spatial ecology and informing

evidence-based conservation practices.

Bibliography

[1] P. Abrams, *The theory of limiting similarity*, Annual Review of Ecology and Systematics **14** (1983), 359–376.

[2] M. Ackermann and M. Doebeli, *Evolution of niche width and adaptive diversification*, Evolution **58** (2004), no. 12, 2599–2612.

[3] E. M. Baptestini, M. A. M. De Aguiar, D. I. Bolnick, and M. S. Araújo, *The shape of the competition and carrying capacity kernels affects the likelihood of disruptive selection*, Journal of Theoretical Biology (2009).

[4] Ali Beykzadeh, *Multi-patch laplace dispersal across biased interfaces*, MSc Thesis, University of New Brunswick, 2019.

[5] Ali Beykzadeh and James Watmough, *An explicit formula for a dispersal kernel in a patchy landscape*, bioRxiv (2019), 680256.

[6] L. Eigentler and J. A. Sherratt, *Long-range seed dispersal enables almost stationary patterns in a model for dryland vegetation*, Journal of Mathematical Biology **86** (2023), no. 15.

[7] Omar Abdul Halim and Mohammad El Smaily, *Asymptotic regimes of an integro-difference equation with discontinuous kernel*, Journal of Dynamics and Differential Equations (2023), 1–15.

[8] Sarah E Lester and Benjamin S Halpern, *Biological responses in marine no-take reserves versus partially protected areas*, Marine Ecology Progress Series **367** (2008), 49–56.

[9] F Lutscher, E Pachepsky, and M Lewis, *The effect of dispersal patterns on stream populations*, SIAM Review **47** (2005), no. 4, 749–772.

[10] Frithjof Lutscher, *Integrodifference equations in spatial ecology*, ch. 1, Springer, 2019.

[11] ———, *Integrodifference equations in spatial ecology*, ch. 3, Springer, 2019.

[12] Gabriel Andreguetto Maciel and Frithjof Lutscher, *How individual movement response to habitat edges affects population persistence and spatial spread*, The American Naturalist **186** (2021), no. 2, E000–E000.

[13] Matteo Marcantonio, Raluca Voda, Daniele Da Re, Quentin Igot, Roger L. H. Dennis, Aurélien Vielfaure, Sophie O. Vanwambeke, and Caroline M. Nieberding, *The effect of habitat on insect movements: Experimental evidence from wild-caught butterflies*, Insects **14** (2023), no. 9.

[14] Jeffrey Musgrave, *Integrodifference equations in patchy landscapes*, PhD Thesis, Université d'Ottawa/University of Ottawa, 2013.

[15] Jeffrey Musgrave and Frithjof Lutscher, *Integrodifference equations in patchy landscapes : I. Dispersal Kernels.*, Journal of Mathematical Biology **69** (2014), no. 3, 583–615.

[16] Michael G Neubert and Mark Kot, *Properties of some density-dependent integrodifference equation models for populations without a seed bank*, Theoretical Population Biology **40** (1991), no. 2, 194–211.

[17] Michael G Neubert, Mark Kot, and Mark A Lewis, *Dispersal and pattern formation in a discrete-time predator-prey model*, Theoretical population biology **48** (1995), no. 1, 7–43.

[18] RFG Ormond, MA Gore, et al., *No-take zones: does behaviour matter?*, (2005).

[19] Otso Ovaskainen and Stephen J Cornell, *Biased movement at a boundary and conditional occupancy times for diffusion processes*, Journal of Applied Probability **40** (2003), no. 3, 557–580.

[20] Nick T Shears, Roger V Grace, Natalie R Usmar, Vince Kerr, and Russell C Babcock, *Long-term trends in lobster populations in a partially protected vs. no-take marine park*, Biological conservation **132** (2006), no. 2, 222–231.

[21] Sam Subbey, Jennifer A. Devine, Ute Schaarschmidt, and Richard D.M. Nash, *Modelling and forecasting stock–recruitment: current and future perspectives*, ICES Journal of Marine Science **71** (2014), no. 8, 2307–2322.

[22] Rob W Van Kirk and Mark A Lewis, *Integrodifference models for persistence in fragmented habitats*, Bulletin of Mathematical Biology **59** (1997), no. 1, 107–137.

[23] Heran Zhang, Nan Shen, Yafeng Li, Cheng Hu, and Peng Yuan, *Source, transport, and toxicity of emerging contaminants in aquatic environments: A review on recent studies*, Environmental Science and Pollution Research **30** (2023), 121420–121437.

Vita

Candidate's full name: Ali Beykzadeh

University attended:

Master of Science in Mathematics (2020)

University of New Brunswick, Fredericton, NB

Thesis: Multi-patch Laplace Dispersal across Biased Interfaces

Supervisor: Dr. James Watmough

Master of Pure Mathematics (1997)

Ferdowsi University, Iran

Thesis: A characteristic for 3-Engel groups

Supervisor: Dr. MRR Moghaddam

Bachelor of Science in Mathematics (1995)

University of Birjand, Iran

Recent Conference Presentations:

Critical Gap Size, The British Applied Mathematics Colloquium

Newcastle University, UK (2024)

Multi-patch Laplace Kernel, Great Lakes Mathematical Physics Meeting

Michigan State University, USA (2024)

Critical Gap Size for Stable Populations in Patchy Environments, Canadian Applied and Industrial Mathematics Society, Queen's University, Kingston ON (2024)